1521-009X/12/4009-1677–1685$25.00
DRUG METABOLISM AND DISPOSITION
Vol. 40, No. 9
44792/3785809

DMD 40:1677–1685, 2012

Development of a Carbon-14 Labeling Approach to Support Disposition Studies with a Pegylated Biologic[S]

Haiqing Wang, Lifei Wang, Kai Cao, Stuart L. Emanuel, Paul Morin, Zheng Lin, Guoxiang Shen, Jennifer Hosbach, Donglu Zhang, Samuel Bonacorsi, A. David Rodrigues, and Zheng Yang

Pharmaceutical Candidate Optimization (H.W., L.W., G.S., D.Z., A.D.R., Z.Y.) and Departments of Chemistry (K.C., S.B.), Biology (S.L.E., J.H.), and Protein Science and Structure (P.M., Z.L.), Bristol-Myers Squibb Research and Development, Princeton, New Jersey

Received February 6, 2012; accepted May 24, 2012

ABSTRACT:

Although it is widely accepted that one can extend the pharmacokinetic half-life of a therapeutic protein by covalent conjugation with polyethylene glycol (PEG), the disposition properties of such biologics have not yet been fully evaluated. Therefore, a novel [^{14}C]-labeling method was developed that can be applied to a biologic conjugated with PEG through a maleimide-cysteine reaction. The method was used to study the tissue and tumor distribution of a PEGylated Adnectin, a recombinant protein derived from the 10th type III domain of fibronectin, in nude mice bearing human xenograft tumors. The PEGylated Adnectin contained a 40-kDa branched PEG (P40B) that was labeled with [^{14}C] at the linker region between the PEG and Adnectin, without compromising cellular activity and plasma half-life in mice. After a single intravenous or intraperitoneal dose (33 mg/kg, 1.7 μCi per mouse) of [^{14}C]-P40B-Adnectin, quantitative whole-body autoradiography analysis revealed that the liver had the highest uptake of the radioactivity among nontumor tissues, followed by the kidneys and lung. The muscle and brain showed the least penetration of the radioactivity among all tissues examined. In addition, the [^{14}C]-P40B-EI-tandem penetrated into the tumor tissue, although the extent of accumulation was largely dependent on tumor type. Therefore, it was possible to assess the tissue distribution of a PEGylated biologic after it had been [^{14}C] labeled using the novel method described herein.

Introduction

For most therapeutic proteins, it is known that one can extend the pharmacokinetic half-life, and hence reduce the dosing frequency, by covalent conjugation with polyethylene glycol (PEG). The PEG moiety increases the hydrodynamic radius of the protein and shields it from the immune system, thus reducing the potential for immunogenicity. A larger hydrodynamic radius also may slow renal excretion, prolong half-life, and shield the protein from various proteolytic enzymes (Gaberc-Porekar et al., 2008; Bailon and Won, 2009; Jevsevar et al., 2010). To date, nine "PEGylated" biologics have been approved for clinic use, with many others currently under development. The majority of commercial PEGylated biologics are recombinant human proteins, such as PEG-interferons for the treatment of hepatitis C. Recently, certolizumab pegol (Cimzia), a PEGylated anti-TNFα antibody fragment (Fab), was approved for the treatment of rheumatoid arthritis and Crohn's disease (Veronese and Mero, 2008). The approval of Cimzia demonstrated the potential of PEGylated biologics as an alternative to conventional therapeutic monoclonal antibodies.

Various protein scaffolds have emerged as a new generation of biologics complementing existing therapeutic antibodies for the treatment of cancer and other chronic disorders. The protein scaffolds are small proteins consisting of a natural backbone derived from human proteins and a flexible targeting domain that is engineered to specifically recognize the therapeutic target of interest (Skerra, 2007; Gebauer and Skerra, 2009). For example, Adnectins are a class of protein scaffolds derived from the 10th type III domain of human fibronectin, an extracellular protein abundant in human serum and the extracellular space. By changing the amino acid sequence of three targeting loops but keeping the scaffold intact, these small proteins (~10 kDa) can bind to specific disease targets with an affinity and specificity comparable to or better than those of antibodies (Emanuel et al., 2011; Lipovsek, 2011). To prolong the residence time of these small protein scaffolds in the body, a variety of novel approaches, such as Fc fusions and albumin binding, are being tested (Gay et al., 2010; Hopp et al., 2010). Nevertheless, PEGylation is still the most reliable and established technology for the extension of pharmacokinetic half-life. For example, the plasma half-life of CT-322, an Adnectin conjugated with a 40-kDa branched PEG, is ~64 h in cancer patients (Tolcher et

Article, publication date, and citation information can be found at http://dmd.aspetjournals.org.
http://dx.doi.org/10.1124/dmd.112.044792.
[S] The online version of this article (available at http://dmd.aspetjournals.org) contains supplemental material.

ABBREVIATIONS: PEG, polyethyleneglycol; BMPS, *N*-(β-maleimidopropyloxy)succinimide; EGFR, epidermal growth factor receptor; EI-tandem, anti-EGFR and anti-IGF-1R tandem Adenctin; ELISA, enzyme-linked immunosorbent assay; IGF-1R, insulin-like growth factor 1 receptor; Ni-NTA, nickel-nitrilotriacetic acid; P40B, two-branch 40-kDa PEG; P40B-NH_2, two-branch 40-kDa PEG-propylamine; QWBA, quantitative whole-body autoradiography; PAGE, polyacrylamide gel electrophoresis; ID/g, injected dose per gram of tissue; PET, positron emission tomography; ^{125}I, iodine-125; HPLC, high-performance liquid chromatography.

al., 2011). The half-life is longer (~64 vs. 1–5 h) than that of non-PEGylated proteins, such as rhGM-CSF (18 kDa), rhIL-3 (15 kDa), and rhIFN-α2a (19 kDa) (Taguchi, 1986; Hovgaard et al., 1992, 1994).

Although it has been widely accepted that the pharmacokinetics of PEGylated biologics is mostly driven by the size of PEG, the disposition properties of such biologics have not yet been fully evaluated. This is possibly due to the difficulties of quantifying PEGylated biologics in different tissues. For example, several labeling methods are available for protein therapeutics, including iodine-125 (^{125}I) and fluorescent labeling, as well as positron emission tomography (PET) tracers (Niu et al., 2009; Hoeben et al., 2011). However, these methods inevitably change the overall structure of the biologic in question. In most cases where the random conjugation is used as the cross-linking chemistry, the resulting product contains heterogenous species, and there is an increased risk that biological and pharmacokinetic properties are altered. In addition, the radionuclide-conjugated biologics require immediate in vivo assessment because of possible radiolysis during storage and the short half-life of the PET tracers. The need for special laboratory protection and instrumentation further complicates disposition studies using the aforementioned labeling approaches. Therefore, a sensitive but convenient labeling method has been sought to support distribution studies with PEGylated biologics. Such distribution data would be useful and enable one to assess differential uptake into target and nontarget (e.g., clearance) tissues and further support efficacy and toxicity assessment.

Toward this end, a novel [^{14}C]-labeling method was developed that can be applied to any protein scaffold conjugated with a PEG via a cysteine residue. Compared with the existing labeling methods, this approach is easy to use. In addition, the labeled molecule shares the same structure as the nonlabeled version and is generally stable because of the [^{14}C] label as a low-energy β-emitter with a long half-life. It was possible to subsequently apply the approach to a 40-kDa branched PEGylated Adnectin (P40B-EI-tandem) that targets both EGFR and IGF-1R (Fig. 1). The antitumor efficacy of the P40B-EI-tandem was demonstrated in various human xenograft tumor models that express EGFR and/or IGF-1R. In the present study, the tissue distribution and tumor uptake of the P40B-EI-tandem was investigated using QWBA after a single intravenous and intraperitoneal dose of [^{14}C]-P40B-EI-tandem.

Materials and Methods

Reagents. All commercial reagents used for synthesis were purchased from Sigma-Aldrich (St. Louis, MO). 1,4-[^{14}C]-Labeled maleic acid (55 mCi/mmol) was obtained from PerkinElmer Life and Analytical Sciences (Waltham, MA). Ecolite scintillation mixture was obtained from MP Biomedicals (Solon, OH). A 40-kDa branched PEG-propylamine (P40B-NH_2) and a maleimide-activated 40-kDa branched PEG (for synthesis of the nonlabeled agent) were purchased from NOF America Corporation (White Plains, NY). Disposable G-25 PD-10 columns and Hi-Trap SP columns were obtained from GE Healthcare Bio-Sciences (Little Chalfont, Buckinghamshire, UK). Ni-NTA agarose resin was purchased from QIAGEN (Valencia, CA), and Sartobind Q 75 filters were acquired from Sartorius Stedim Biotech (Aubagne, France).

Synthesis of [^{14}C]-Labeled Cross-Linker. Preparation of [^{14}C]-labeled cross-linker ([^{14}C]-BMPS) was accomplished in two steps as shown in Fig. 2A. The starting materials 3-aminopropanoic acid (98 mg, 1.1 mmol) and [1,4-^{14}C]-maleic acid (118 mg, 1.0 mmol; specific activity, 55 mCi/mmol) were dissolved in 3.5 ml of dioxane and heated to 110°C for 18 h in the presence of phosphorouspentoxide (P_2O_5, 156 mg, 1.1 mmol). The reaction mixture was then filtered while it was hot. The crude product mixture was purified on a 21.2 × 250 mm Synergy Hydro-RP column (Phenomenex, Torrance, CA), using the following separation condition: flow rate, 16 ml/min; UV wavelength, 220 nm; mobile-phase solvent A, water (0.1% trifluoroacetic acid); mobile-phase solvent B, acetonitrile (0.1% trifluoroacetic acid); flow gradient, 10% B in A at 0 min, 40% B in A at 10 min, 95% B in A at 15 min, 10% B at 20 min; retention time, 8.4 min. 4-([1,4-14C]-Maleimido)propanoic acid (34 mg) was obtained after evaporation (Alagic et al., 2005). The dried product (34 mg, 0.20 mmol) and *N*-hydroxysuccinimide (29 mg, 0.25 mmol) were dissolved in cooled ethyl acetate (1 ml) submerged in an ice bath. *N*,*N*′-Diisopropylcarbodiimide (0.062 ml, 0.40 mmol) was added to the solution, and the mixture was stirred for 3 h. Dichloromethane (20 ml) was then added to the reaction mixture, followed by filtration, to remove urea. The organic layer was then washed with water (5 ml × 2), dried over Na_2SO_4, and filtered. The product ([^{14}C]-BMPS, 56 mg, 12 mCi) was obtained after evaporation, and its specific activity was determined by gravimetric analysis (56 mCi/mmol).

Purification of EI-Tandem. The construction and characterization of the EI-tandem was reported previously (Emanuel et al., 2011). The 23-kDa recombinant protein was produced by covalently linking an EGFR-binding Adnectin to the C terminus of an IGF-IR-binding Adnectin using a glycine-

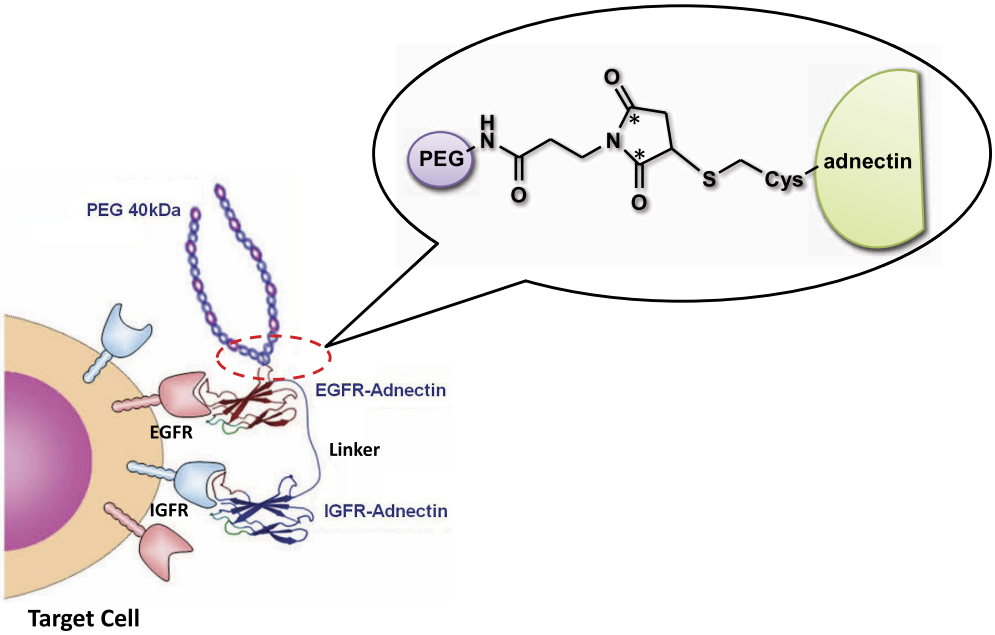

FIG. 1. Schematic representation of a 40-kDa branched PEGylated Adnectin (P40B-EI-tandem). The tandem Adnectin targets both human EGFR and IGF-1R, and the structure of the cross-linker (BMPS) between the Adnectin and PEG is shown.

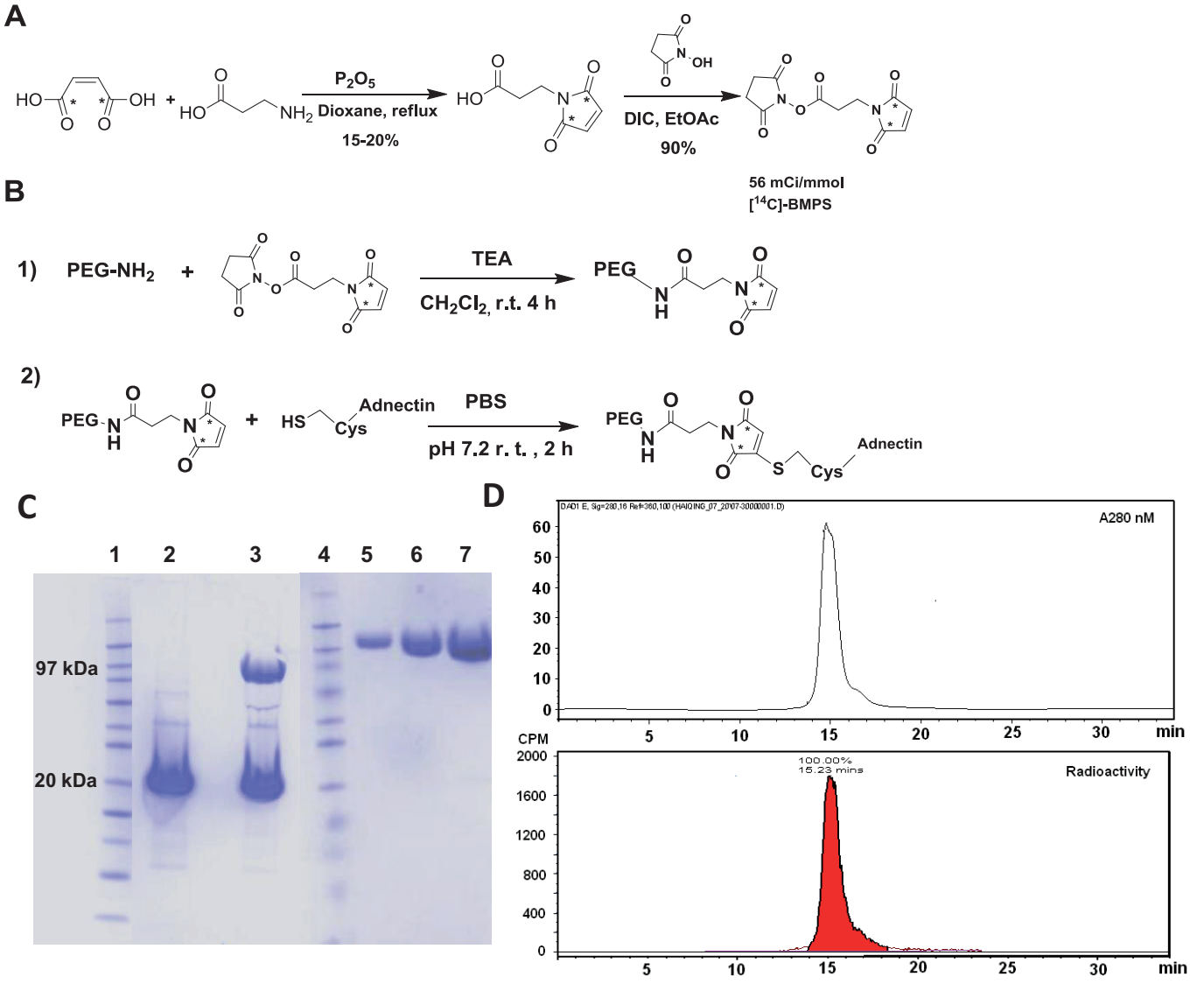

FIG. 2. Synthesis and purification of the [^{14}C]-P40B-EI-tandem. A, synthesis of [^{14}C]-BMPS. The asterisk on the maleimide pyrrole ring indicates the position of the [^{14}C] label. B, synthetic scheme of [^{14}C]-P40B-EI-tandem. C, purity of [^{14}C]-P40B-EI-tandem revealed by SDS-PAGE. Lanes 1 and 4, molecular mass marker; lane 2, purified EI-tandem eluted from Ni-NTA affinity column; lane 3, EI-tandem upshifted to 100 kDa after conjugation with [^{14}C]-maleimide-P40B; lanes 5–7, 2, 6, and 12 μg of purified [^{14}C]-P40B-EI-tandem, respectively. D, analysis of purity and specific radioactivity of [^{14}C]-P40B-EI-tandem by size-exclusion gel filtration chromatography. Top, UV trace of HPLC elution profile at A280 nm; bottom, radioactivity trace of the same elution profile. TEA, triethylamine; EtOAc, ethyl acetate; DIC, *N,N'*-diisopropylcarbodiimide.

serine linker (Fig. 1). The protein was expressed as a C-terminus His_6-tag fusion for affinity purification. To conjugate with PEG, a serine-to-cysteine mutation was introduced into the protein near the C terminus. The protein was overexpressed in *Escherichia coli* and purified using Ni-NTA agarose resin following the manufacturer's instructions. The purified EI-tandem was eluted from the Ni-NTA resin using Na_2HPO_4 (20 mM, pH 8.0) buffer containing 400 mM NaCl and 400 mM imidazole and immediately coupled with [^{14}C]-labeled, maleimide-activated 40-kDa branched PEG ([^{14}C]-maleimide-PEG) as described below.

Synthesis of [^{14}C]-Maleimide-PEG and Subsequent PEGylation. The reaction procedure of [^{14}C]-maleimide-PEG synthesis and the subsequent PEGylation with purified EI-tandem are outlined in Fig. 2B. [^{14}C]-BMPS (5 mg, 20 μmol, 1 mCi) was dissolved in 4 ml of CH_2Cl_2 and transferred to a glass vial containing 40-kDa branched PEG-propylamine (P40B-NH_2, 160 mg, 4 μmol) powder. After the addition of triethylamine (14 μl, 100 μmol), the reaction mixture was stirred at room temperature for 4 h. The solvent was then evaporated to dryness under a stream of nitrogen. The residue was resuspended in a 2-ml Tris buffer (10 mM, pH 7.0) to quench the amine-coupling reaction. The unreacted [^{14}C]-BMPS and other small-molecule byproducts were removed by applying the mixture onto a G-25 PD-10 column pre-equilibrated with the Tris buffer (10 mM, pH 7.0). The eluate containing [^{14}C]-maleimide-PEG was conjugated with the freshly purified EI-tandem, through a maleimide and cysteine reaction to yield [^{14}C]-P40B-EI-tandem. The reaction mixture was incubated at room temperature for 2 h. Progress of the PEGylation was confirmed by SDS-PAGE (Fig. 2C). The reaction mixture was dialyzed into a 50-mM NaAc buffer, pH 4.5, for purification using cation exchange chromatography (see below).

SDS-PAGE. The PEGylated and non-PEGylated EI-tandem were separated using a Novex mini-gel electrophoresis system (Invitrogen, Carlsbad, CA). The protein samples were denatured after adding lithium dodecyl sulfate sample buffer and heating at 70°C for 5 min. Samples (15–20 μl) were subsequently loaded onto a precast 10% NuPAGE Bis-Tris Gel and subjected to electrophoresis in SDS-MES (2-[*N*-morpholino] ethane sulfonic acid) running buffer at 200 V for 45 min. Gels were stained using Simply Blue Safestain (Invitrogen). The molecular weight of the protein bands was estimated by comparing with the Novex Sharp Protein Standards. All reagents for SDS-PAGE were obtained from Invitrogen.

Purification of [^{14}C]-P40B-EI-Tandem. [^{14}C]-P40B-EI-tandem was purified by cation exchange chromatography. In brief, the dialyzed mixture was clarified by centrifugation and loaded onto a HiTrap sulfopropyl Sepharose column pre-equilibrated with the 50-mM NaAc buffer at pH 4.5 (buffer A). The column was washed with buffer A to remove the unconjugated PEG. The PEGylated versus non-PEGylated proteins were separated and eluted with a linear gradient of 0 to 0.5 M NaCl in buffer A. The fractions containing [^{14}C]-P40B-EI-tandem were pooled, concentrated, and buffer exchanged to Dulbecco's PBS buffer, pH 7.2. Lipo-polysaccharides were removed with Sartobind Q charged membranes following the manufacturer's protocol. The purity of [^{14}C]-P40B-EI-tandem was checked by SDS-PAGE (Fig. 2C) and gel filtration analysis using a Shodex KW-803 size exclusion column (Showa Denko America, Inc., New York, NY) connected to a HPLC system with a radio-HPLC detector (Fig. 2D).

Concentration and Radioactivity Determination. The concentration of PEGylated and non-PEGylated proteins was determined by A280/A260 measurement using Nanodrop 1000 (Thermo Fisher Scientific, Waltham, MA). Because PEG does not have a UV absorbance, the mass of the PEG portion in the PEGylated protein was not considered. Consequently, a molecular mass of 23 kDa (protein only), rather than that of 63 kDa (PEG plus protein), was used to convert mass unit (milligrams per milliliter) to molar unit (nanomolar or micromolar). To determine the total radioactivity of [^{14}C]-P40B-EI-tandem, the PEGylated protein (1–10 μl) was diluted with Ecolite scintillation mixture, followed by radioactivity counting on a Beckman LS6000 liquid scintillation counter (Beckman Coulter, Fullerton, CA). The specific activity was calculated to be 2.5 μCi/mg protein (55 mCi/mmol).

Inhibition of IGF-IR/EGFR Phosphorylation in H292 Cells. H292 cells (65,000 cells/well) were plated in 96-well plates and incubated overnight. After 24 h, cells were washed once and incubated for 24 h in serum-free medium. Serial dilutions of either [^{14}C]-labeled or nonlabeled P40B-EI-tandem were added, and cells were incubated for 3 h. Cells were stimulated with 100 ng/ml IGF-I or EGF for 10 min at 37°C. Medium was removed, and cells were lysed in a 100-μl cell lysis buffer as described for immunoblotting (Emanuel et al., 2008, 2011). After a 15-min incubation at room temperature, the lysate was subjected to an ELISA measuring phospho-IGF-IR (Tyr1131), or phospho-EGFR (Tyr1068), according to the manufacturer's procedure (Cell Signaling Technology, Danvers, MA).

Animal Preparation and Dosing. Female athymic nude mice 5 to 6 weeks of age were obtained from Harlan (Indianapolis, IN) and quarantined for 3 weeks before their use in experiments. Animals were provided food and water ad libitum and were cared for according to the Association for Assessment and Accreditation of Laboratory Animal Care International and Bristol-Myers Squibb guidelines. Tumors were propagated by subcutaneous implantation of 1-mm^3 fragments in nude mice. The RH41 tumor was implanted in the right hind flank 2 weeks before the implantation of the H292 tumor in the left hind flank. When the tumor sizes reached 300 mm^3, the mice were dosed intravenously or intraperitoneally with 33 mg/kg [^{14}C]-P40B-EI-tandem (total radioactivity, 1.7 μCi per mouse). Two mice from each group were sacrificed at 2, 24, 48, and 53 h after intravenous dosing or 8, 48, and 53 h after intraperitoneal dosing. The serum samples were collected for exposure analysis. One mouse each after intravenous (2, 24, and 53 h) and intraperitoneal (8 and 53 h) dosing was used for QWBA analysis.

Analysis of [^{14}C]-P40B-EI-Tandem in Serum. The serum concentration of [^{14}C]-P40B-EI-tandem was determined by ELISA. The recombinant biotinylated IGF-1R (Bristol-Myers Squibb Co., Stamford, CT) was coated on a 96-well streptavidin plate at a final concentration of 0.5 μg/ml. [^{14}C]-P40B-EI-tandem from mouse serum was captured onto the plate. After a washing step, the captured [^{14}C]-P40B-EI-tandem was detected by an anti-PEG monoclonal rabbit antibody (Epitomics, Burlingame, CA) that was subsequently detected by a sulfo tag-conjugated anti-rabbit polyclonal antibody. The concentrations were calculated based on the electrochemiluminescence of the sample compared with a four-parameter fit of a standard curve. The dynamic range of the assay is 0.8 to 200 nM, with a lower limit of quantification of 1 nM.

Analysis of Serum Concentration of Radioactivity. An aliquot of a 10-μl serum sample was diluted 10-fold to 100 μl. The diluted serum (20 μl) was added to a scintillation vial containing 5 ml of Ecolite scintillation mixture, followed by radioactivity counting on a Beckman LS6000 liquid scintillation counter (Beckman Coulter). The resulting disintegrations-per-minute values were converted to the radioactivity concentration using the equation below:

$$[\text{Radioactivity}](\mu\text{M}) = \frac{\text{dpm} \times 10^6}{2\mu\text{l} \times 2.22 \times 10^6\left(\frac{\text{dpm}}{\mu\text{Ci}}\right) \times 2.5\left(\frac{\mu\text{Ci}}{\text{mg}}\right) \times 23{,}000(\text{Da})} \quad (1)$$

where 2 μl is the serum volume, 2.22×10^6 dpm/μCi is the conversion factor, 2.5 μCi/mg is the specific activity, and 23,000 Da is the molecular mass.

QWBA. The whole-body sections of the frozen mouse carcasses were taken at 40 μm thick in the sagittal plane and captured on an adhesive tape (Scotch Tape 8210; 3M Ltd., St. Paul, MN) at −20°C. Sections at various levels were collected to include the major tissues and tumors and dried in the cryomicrotome at −20°C for 48 h. The sections of each mice were mounted on a cardboard, covered with a thin plastic wrap, and exposed along with a calibration standard of [^{14}C]-glucose at 14 different concentrations (ranging from ~0 to 0.8 μCi/g) to a [^{14}C]-sensitive phosphor imaging plate (Fuji Biomedical, Stamford, CT). The exposure experiment was conducted in light-tight exposure cassettes for 5 days at room temperature in a lead-shielding box. After exposure, the imaging plates were scanned using the Fuji FLA-3000 image acquisition system (Fuji Biomedical). The image files were processed using MCID image analysis software (version 7.0; Imaging Research, St. Catherines, ON, Canada), and a standard curve was constructed from the integrated response and the radioactivity concentrations of the [^{14}C] calibration standard. The lower limit of quantification was determined to be 0.5 nCi/g.

Results

Design and Preparation of [^{14}C]-P40B-EI-Tandem. The diagram structure of the P40B PEGylated EI-tandem is illustrated in Fig. 1. It was constructed as two tandemly connected Adnectins with the N-terminus unit specifically bound to IGF-IR and the C-terminus unit bound to EGFR. A serine-to-cysteine mutation was introduced near the C terminus to enable site-specific PEGylation. It was shown that the binding affinities of the EI-tandem to IGF-1R and EGFR were not compromised after the mutation (Emanuel et al., 2011). The EI-tandem Adnectin and PEG were covalently linked via a thioether and an amide bond. To form this linkage, a bifunctional cross-linker (BMPS) was used (Fig. 1). The linker reacted with the 40-kDa branched PEG-propylamine (P40B-NH_2) via a succinimide-amine coupling reaction and with cysteine in the EI-tandem Adnectin via a maleimide-thiol reaction. The synthesis of the bifunctional cross-linker is described under *Materials and Methods* using 1,4-[^{14}C]-maleic acid as the starting material to introduce the [^{14}C] label (Fig. 2A). The specific activity of the resulting [^{14}C]-BMPS was 55 mCi/mmol.

The [^{14}C]-P40B-EI-tandem was prepared via a two-step process (Fig. 2B). First, the P40B-NH2 was conjugated with an excess amount of [^{14}C]-BMPS in CH_2Cl_2 under basic conditions by the addition of triethylamine. After completion of the reaction, the organic solvent was removed via evaporation, and the product was dissolved in a PBS buffer. The product, [^{14}C]-maleimide-PEG, shares the same structure as the nonradiolabeled version available from NOF America Corporation for the routine site-specific PEGylation of proteins. The residual [^{14}C]-BMPS was removed by ultrafiltration before the subsequent conjugation with the EI-tandem Adnectin. In parallel with the [^{14}C]-maleimide-PEG synthesis, the EI-tandem Adnectin was purified by subjecting *E. coli* lysate to Ni-NTA affinity chromatography. To avoid intermolecule disulfide formation, the purified protein was immediately conjugated with the [^{14}C]-maleimide-PEG through the maleimide-thiol reaction to yield [^{14}C]-P40B-EI-tandem. The PEGylation reaction was monitored by SDS-PAGE (Fig. 2C), where the Coomassie Blue-stained protein band was shifted from below 30 kDa

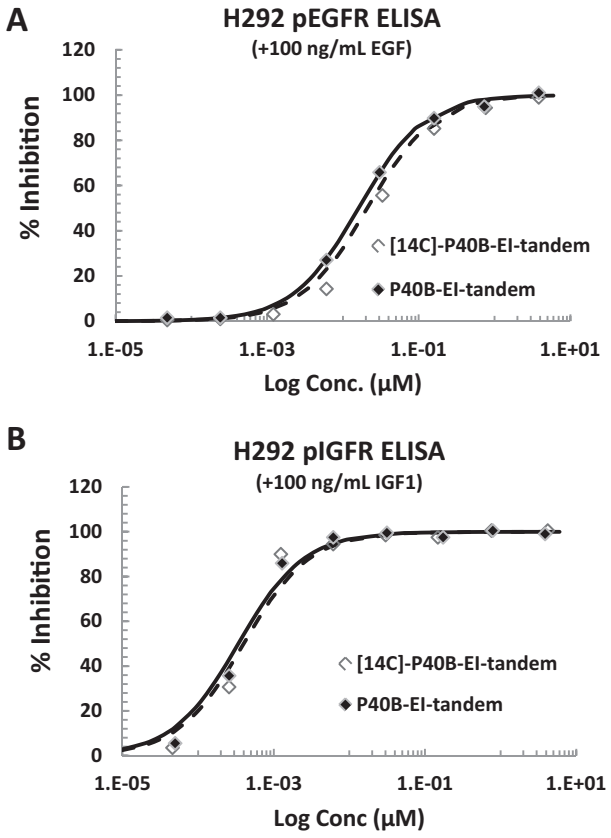

FIG. 3. In vitro cellular activity of [^{14}C]-P40B-EI-tandem. A, inhibition of EGFR phosphorylation in H292 cells. B, inhibition of IGF-IR phosphorylation in H292 cell. Log Conc., Log concentration.

for the EI-tandem Adnectin to above 100 kDa after PEGylation. The apparent higher mass is typical of a PEGylated protein on a SDS-PAGE gel (Sato, 2002). The PEGylated product, [^{14}C]-P40B-EI-tandem, was further purified on a HiTrap cation exchange column to ensure electrophoretic homogeneity (Fig. 2C). The purity and specific radioactivity were verified by size-exclusion chromatography (Fig. 2D). Both UV (A280 nm) and radioactivity traces showed a single peak eluted at 15 min, suggesting the radioactivity was nearly 100% in the final purified product. Lipopolysaccharides were subsequently removed from the final purified PEGylated protein by the Sartobind Q 75 filter. The specific activity was determined to be 2.5 μCi/mg protein (55 mCi/mmol).

The nonradiolabled P40B-EI-tandem was prepared following the same procedure as the [^{14}C]-radiolabeled version, except that the purified EI-tandem was directly conjugated with the maleimide-activated PEG purchased from NOF America Corporation.

Inhibition of Receptor Phosphorylation by the [^{14}C]-P40B-EI-Tandem. The inhibitory potency of [^{14}C]-P40B-EI-tandem was evaluated in the H292 lung cancer cell line. The H292 cell line was selected because of its high-level expression of both EGFR and IGF-1R and sensitivity to growth inhibition by anti-EGFR agents. As shown in Fig. 3, A and B, [^{14}C]-P40B-EI-tandem inhibited EGF-stimulated EGFR phosphorylation with an IC_{50} of 23 nM and blocked IGF-stimulated IGF-1R phosphorylation with an IC_{50} of 0.3 nM. The inhibitory potency was equivalent to the nonradiolabeled P40B-EI-tandem tested in the same experiment (Fig. 3, A and B) and nearly identical to the previously reported IC_{50} values of 31 nM (blocking EGFR) and 0.2 nM (blocking IGF-1R) (Emanuel et al., 2011). The results clearly demonstrated that the [^{14}C] label introduced in the linker region did not affect the cellular potency of the PEGylated EI-Adnectin.

Pharmacokinetics and Tissue Distribution of [^{14}C]-P40B-EI-Tandem in H292 and RH41 Tumor-Bearing Mice. The H292 and RH41 cell-derived tumor fragments were implanted in athymic mice on either side of the hind flank. In contrast to H292 cells that are sensitive to both EGFR and IGF-1R signaling, the proliferation of RH41 Ewing sarcoma cells is driven predominantly by IGF-1R signaling and is not sensitive to EGFR blockade. When both tumors had grown to ~300 mm^3, [^{14}C]-P40B-EI-tandem was administered intravenously or intraperitoneally (33 mg/kg, 1.7 μC per mouse).

The serum concentration of [^{14}C]-P40B-EI-tandem after intravenous and intraperitoneal administration was determined by ELISA. After the intraperitoneal administration, the average concentrations after dose adjustment were 0.27 and 0.066 $\mu M \cdot mg^{-1} \cdot kg^{-1}$ at 8 and 48 h, respectively (Table 1). The dose normalized exposures were in line with those of the nonlabeled P40B-EI-Adnectin after 10 and 100 mg/kg i.p. administration, which were 0.27 to 0.33 and 0.044 to 0.077 $\mu M \cdot mg^{-1} \cdot kg^{-1}$ at 8 and 48 h, respectively (Emanuel et al., 2011). The comparable exposures suggest similar in vivo stability of the [^{14}C]-labeled and nonlabeled P40B-EI-Adnectin, consistent with the in vitro findings.

The serum concentrations of radioactivity were also measured (Table 1). The radioactivity concentrations were systematically ~2-fold (1.7–2.4-fold) higher than the concentrations determined by the ELISA method, which, we believe, is largely due to the systemic error between the two analytical methods. Nevertheless, there seemed to be a trend of increase in the ratios from 1.7-fold at 2 and 24 h to 2.4-fold at 53 h, indicating the protein portion of the PEGylated tandem EI-Adnectin may be degraded and/or inactivated over the study duration. Assuming 100% of the radioactivity is from the intact P40B-

TABLE 1

Serum concentrations determined by radioactivity and ELISA methods after intravenous and intraperitoneal administration of [^{14}C]-P40B-EI-Adenctin (33 mg/kg)

Time	[^{14}C]-P40B-EI-Adnectin						P40B-EI-Adnectin[a]	
	33 mg/kg i.v.			33 mg/kg i.p.			10 mg/kg i.p.	100 mg/kg i.p.
	Radioactivity[b]	ELISA[b]	Concentration Ratio Radioactivity/ELISA	Radioactivity[b]	ELISA[b]	Concentration Ratio Radioactivity/ELISA	ELISA	
	μM			μM	μM ($\mu M \cdot mg^{-1} \cdot kg^{-1}$)		μM ($\mu M \cdot mg^{-1} \cdot kg^{-1}$)	
2 h	14, 16	7.8, 9.8	1.7					
8 h				14, 15	8.7, 9.3 (0.27)[c]	1.6	3.3 ± 0.1 (0.33)[c]	27 ± 2.6 (0.27)[c]
24 h	7.8, 7.2	4.5, 4.3	1.7					
48 h	4.7, 3.9	2.1, 1.7	2.3	5.0–5.2	2.0, 2.4 (0.066)[c]	2.3	0.4 ± 0.04 (0.04)[c]	7.7 ± 1.1 (0.077)[c]
53 h	3.9, 4.0	1.6, 1.7	2.4	3.8, 4.3	1.5, 1.8 (0.05)[c]	2.3		

[a] The exposures of the nonlabeled P40B-EI-Adnectin were first reported by Emanuel et al. (2011).
[b] Concentration from individual mouse.
[c] The data in parentheses are the dose-normalized average concentrations.

EI-Adnectin at 2 h, approximately 30% [(2.4 − 1.7)/2.4 × 100% = 30%] of the radioactivity concentration may come from the circulating PEGylated fragment at 53 h. Further profiling is required to characterize the radioactive species in the serum.

At 2, 24, and 53 h after intravenous dosing, the distribution of radioactivity in mouse tissues was determined by QWBA (Table 2), and the images of the radioactivity distribution are shown in Fig. 4, A–C. At 2 and 24 h, the highest radioactivity appeared in blood, followed by the lung. Significant radioactivity was also observed in the heart, liver, and kidneys. At 53 h, the radioactivity in the liver and kidneys was higher than that in the blood and lung. High radioactivity was also observed in some part of the skin, which is likely due to the comparative binding affinity of the EI-tandem to both mouse and human EGFR (Emanuel et al., 2011). Figure 4E shows the relative radioactivity levels of [^{14}C]-EI-tandem Adnectin in major tissues at 2, 24, and 53 h after intravenous administration into the mice bearing both RH41 and H292 tumors. At each time point, the level of radioactivity in each tissue was normalized by the level in the blood to yield tissue/blood ratios. The ratios increased over time in the liver, kidneys, and bone marrow, indicating the slow uptake of [^{14}C]-P40B-EI-tandem into these tissues. In contrast, the tissue/blood ratios for the lung and heart remained the same from 2 to 53 h, indicating that the distribution of [^{14}C]-P40B-EI-tandem into these tissues reached equilibrium within 2 h after intravenous dosing. At 2 and 24 h, the highest levels of radioactivity were observed in blood. However, at 53 h, the levels in the liver and kidneys were 1.7- and 1.2-fold higher than that in blood, suggesting the accumulation of [^{14}C]-P40B-EI-tandem in both tissues. The muscle and brain had much lower levels of radioactivity compared with other tissues. The highest tissue/blood ratios for the muscle and brain during the study were observed at 53 h (ratios of 0.1 and 0.03, respectively).

Similar tissue distribution patterns were observed after intraperitoneal administration to the mice bearing the same kind of tumors (Supplemental Table S1 and Supplemental Fig. S1A). The tissue/blood ratios increased 5- and 7-fold in the liver and kidneys, respectively, suggesting the substantial uptake of [^{14}C]-P40B-EI-tandem into these tissues over the time interval studied. At 53 h, the levels of radioactivity in the liver and kidneys were 2.0- and 1.3-fold higher than in blood, comparable to the values obtained after intravenous administration. The levels of radioactivity in the lung, heart, and bone marrow were similar, and no accumulation in these tissues was observed. The muscle and brain had the lowest levels of radioactivity among all the tissues analyzed, consistent with the results obtained after intravenous administration.

TABLE 2

Tissue distribution of radioactivity in xenograft mice bearing H292 and RH41 tumors after a single intravenous dose of [^{14}C]-P40B-EI-tandem

Tissues	Radioactivity in Tissue[a]		
	2 h	24 h	53 h
	%ID/g tissue		
Blood (heart)	27.9	14.3	6.2
Tumor (RH41)	1.1	1.9	2.6
Tumor (H292)	5.9	6.1	10.8
Brain	0.5	0.3	0.2
Bone marrow	5.2	3.5	2.1
Heart	9.3	4.3	2.2
Liver	6.8	5.9	10.6
Lung	16.1	8.4	3.6
Kidney (cortex)	6.2	6.8	7.5
Muscle	0.4	0.5	0.5

[a] The radioactivity in the tumors was calculated as the average radioactivity at the rim and in the center. The quantitation limit was 0.03% ID/g tissue.

Tumor Uptake of [^{14}C]-P40B-EI-Tandem. The extent of radioactivity distribution into the RH41 and H292 tumor tissues seemed to be both time and tumor dependent. As shown in Fig. 4D, the radioactivity in both tumors planted in the same mouse increased over time. At 2 and 24 h, the radioactivity located at the rim of the RH41 tumor but penetrated into the tumor 2 days later. In contrast, a significant amount of radioactivity was detected in the H292 tumor as early as 2 h after intravenous administration, and the radioactivity in the H292 tumor was 3- to 5-fold greater than that in the RH41 tumor during the duration of the study (Fig. 4, D and E).

The radioactivity in the tumors was compared with that in blood (Fig. 4E). For the H292 tumor, the tumor/blood radioactivity ratios increased from 0.2 to 0.4 between 2 and 24 h after dose. At 53 h, the accumulation of radioactivity in the H292 tumor became evident (1.7-fold higher than that in blood). However, the tumor/blood radioactivity ratios in the RH41 tumor were less than 1.0 across the study duration, suggesting no accumulation of radioactivity in the tumor.

Similar time- and tumor-dependent uptake of [^{14}C]-P40B-EI-tandem was observed after intraperitoneal administration (Supplemental Table S1 and Fig. S1). At 8 h after dose, the radioactivity in the tumors was lower than that in blood, with H292 and RH41 tumor/blood ratios of 0.3 and 0.1, respectively, indicating a slow tumor penetration of [^{14}C]-P40B-EI-tandem. At 53 h after dose, the accumulation of radioactivity was evident in the H292 tumor, with the tumor radioactivity 2.4-fold higher than that in blood. In contrast, the tumor/blood ratios of RH41 were less than 1.0, suggesting no accumulation of radioactivity in the tumor.

Discussion

Therapeutic biologicals have expanded beyond conventional monoclonal antibodies and recombinant human proteins to include multiple classes of macromolecules (Skerra, 2007; Gebauer and Skerra, 2009). Given the increased variety of scaffolds, numerous strategies have been used to prolong the pharmacokinetic half-life, enhance exposure, and reduce dosing frequency. For example, some biologics are targeted to bind the FcRn receptor and avoid lysozomal digestion. Others are conjugated with PEG or albumin, leading to an increased hydrodynamic radius and decreased renal filtration. Monoclonal antibodies and small protein scaffolds fused with the Fc fragment are examples of the first strategy, whereas the latter is best exemplified by PEGylated biologics or albumin binders (Skerra, 2007; Veronese and Mero, 2008; Bailon and Won, 2009; Gebauer and Skerra, 2009).

Ideally, a therapeutic protein exhibits superior potency and optimal pharmacokinetic properties. However, in reality, the parts of the molecule that govern pharmacokinetics can alter or diminish pharmacologic activity by creating steric hindrance and also impact distribution into target tissues. Conversely, the pharmacologically active parts of the molecule may give rise to accelerated clearance via target-mediated elimination. Therefore, it is important to understand the overall properties of any therapeutic protein and use the information to drive the rational design of viable clinical candidates (Fishburn, 2008). Consequently, there is a need to develop new tools and methods that support the conduct of radiolabel disposition studies. This is especially important when having to assess the uptake of the protein into a target organ or group of cells, link pharmacokinetics to pharmacological activity, support efficacy studies in animal models, and evaluate toxicity in specific organs.

As described herein, it was possible to develop a convenient [^{14}C]-labeling approach for a mono-PEGylated biologic and then assess its tissue distribution in mice. The [^{14}C] label was introduced at the linker region of the PEGylated biologic based on several considerations. First, the synthesis of the [^{14}C]-labeled bifunctional cross-linker

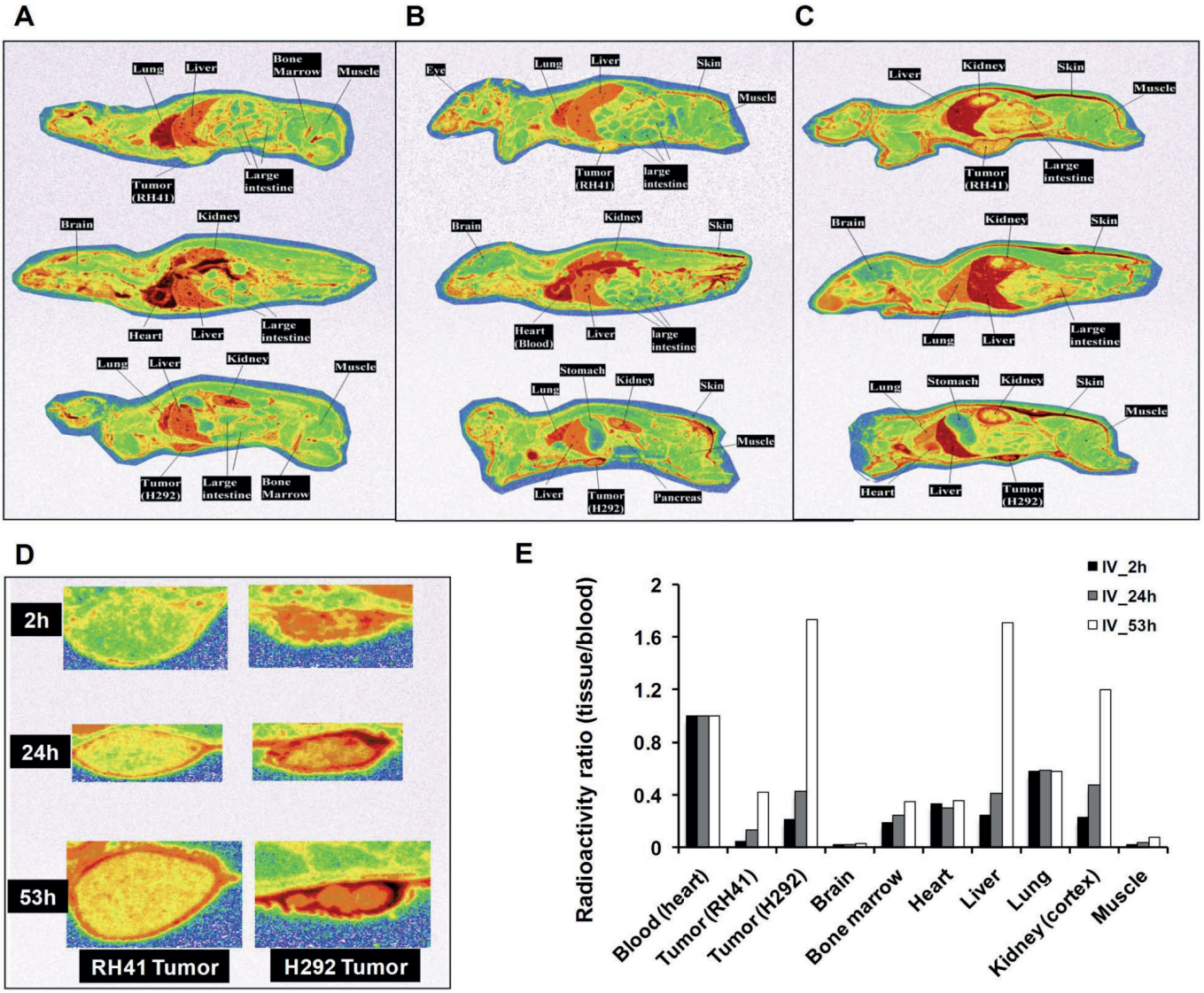

FIG. 4. Tissue distribution and tumor uptake of [^{14}C]-P40B-EI-tandem in H292 and RH41 tumor-bearing mice. A–C, representative whole-body autoradiograms of radioactivity distribution at 2, 24, and 53 h, respectively, after intravenous dosing of [^{14}C]-P40B-EI-tandem (33 mg/kg; 1.7 μCi per mouse). D, uptake of radioactivity into RH41 and H292 tumors at 2, 24, and 53 h after intravenous dosing. E, tissue/blood radioactivity ratios at 2, 24, and 53 h after intravenous (IV) dosing to the tumor-bearing mice.

[^{14}C]-BMPS was straightforward. The reagent is applicable to most site-specific mono-PEGylations through the maleimide-cysteine reaction. Thus, the specific activity will be consistent from batch to batch and among various PEGylated proteins. Second, the [^{14}C] label has little impact on biological activity because the labeled biologic has the same structure as the nonlabeled version. Moreover, [^{14}C] is a low-energy β-emitter that is expected to cause much less radiolysis of the labeled protein compared with [^{125}I] and other similar high-energy radionuclides (Chakrabarti et al., 1996). Finally, although it is feasible to incorporate [^{14}C]-labeled amino acids during protein expression, the resulting radioactive protein would complicate purification and characterization. In addition, [^{14}C] amino acids can be recycled after proteolysis and incorporated into endogenous proteins in the body, which may potentially confound the data interpretation. Therefore, we believe that labeling the linker region is a reasonable approach.

The caveat of the current labeling method is that the radioactivity signal may represent a mixture of both the intact and the degraded PEGylated fragments, as expected from any study using radiolabeled material. In this study, the ratios of the radioactivity over the active P40B-EI-Adnectin concentration seemed to increase ~30% over time, suggesting the presence of the circulating PEGylated fragments. Because the stability of the [^{14}C]-P40B-EI-tandem and the nonlabeled version is similar, the [^{14}C] label could be utilized as a tracer and enable the profiling of sera and tissues.

Although antibodies have been considered as a "silver bullet" for targeted cancer therapy, the delivery of macromolecules to target cells in solid tumors poses a significant challenge. Extensive studies have been conducted in mouse xenograft models to understand the delivery of anti-EGFR antibodies, such as panitumumab and cetuximab, to the solid tumors (Cai et al., 2007; Niu et al., 2009; Nayak et al., 2010a,b; Hoeben et al., 2011). Therefore, it was of interest to characterize the target delivery and disposition of P40B-EI-tandem in mouse xenografts using the [^{14}C]-labeling approach. The H292 and RH41 xenografts were selected for the study based upon the previous results, where the P40B-EI-tandem demonstrated nearly complete tumor growth inhibition (94% tumor growth inhibition) in the H292 xenograft mode, but less than 60% tumor growth inhibition in the RH41 model at the same dose level (100 mg/kg i.p., three times per week) (Emanuel et al., 2011). To understand whether the difference in sensitivity was related to the exposure level of the drug in tumor

tissues, the H292 and RH41 tumors were implanted in the same mice to compare the tumor exposure at the same systemic exposure levels.

After a single intravenous or intraperitoneal dose of [^{14}C]-P40B-EI-tandem, the highest uptake of radioactivity in the H292 and RH41 tumors was 11 and 3.6% of injected dose (ID)/g, respectively, at 53 h after dose. The level is within the range (2–35% ID/g) of the maximum concentrations observed for [^{64}Cu]-1,4,7,10-tetraazacyclododecane-*N*,*N*′,*N*′,*N*″-tetraacetic acid (DOTA)-labeled cetuximab and panitumumab in various EGFR-expressing tumor models (Cai et al., 2007; Niu et al., 2009). This result indicates that the PEGylated EI-tandem may face the same obstacle as the antibodies in penetrating into the tumor because of the hydrodynamic radius of the PEG. Comparing the radioactivity in the two tumor types, at similar systemic exposures, the accumulation in the H292 tumor was higher (3–5-fold) versus the RH41 tumor over the entire study period. The results seemed to correlate well with the better efficacy observed in the H292 tumor-bearing mice. However, it is unknown whether the higher level of accumulation in the H292 tumor was due to the expression of EGFR and IGF-1R in the tumors. Previous PET imaging studies with ceutximab in xenografts showed that the levels of the antibody detected in the tumor tissues did not correlate with the receptor expression levels but may be related to the degree of vasculation of the tumor tissues. This suggests that vessel density and vascular permeability may play an important role in the tumor uptake of macromolecules (Niu et al., 2009). Therefore, immunohistochemical assessment of EGFR and IGF-1R expression levels, as well as analysis of microvascular density markers (e.g., CD31), in the H292 and RH41 tumor tissues is warranted. Such data could prove useful when trying to evaluate possible uptake mechanisms.

The P40B-EI-tandem exhibited comparable binding affinity to mouse and human EGFR in vitro (S. L. Emanuel, unpublished data). Therefore, the distribution of the [^{14}C]-P40B-EI-tandem in mouse tissues may provide insights into the distribution in humans. In mice, the distribution of [^{14}C]-P40B-EI-tandem to the heart and lung was completed within the first 2 h after intravenous administration. However, the radioactivity was slowly absorbed into the liver, kidneys, and tumor tissues. At 53 h, the radioactivity accumulated in the liver was 11% ID/g, 1.7-fold higher than that in blood and representing the highest level among nontumor tissues. Initially, the accumulation of [^{14}C]-P40B-EI-tandem in the liver was thought to be target specific, because a high expression level of EGFR was reported in the mouse liver using the anti-EGFR DOTA affibody (Tolmachev et al., 2010). Moreover, a previous tissue distribution study with the ^{125}I-labeled single-chain bispecific anti-CD19 and CD3 diabody, formatted with 40-kDa PEG, did not show accumulation in the liver (Stork et al., 2009). However, a recent in-house study with a similar P40B-PEGylated protein that neither binds to mouse EGFR nor targets liver-abundant proteins showed similar accumulation in the liver as that of [^{14}C]-P40B-EI-tandem. These results have lead to the hypothesis that the radioactivity accumulation in the liver may not be due to the binding to mouse EGFR but may be related to phagocytosis by liver (Kupffer) cells, similar to PEGylated liposomes (Ishida and Kiwada, 2008).

In conclusion, a novel method has been developed for the [^{14}C] labeling of a PEGylated EI-tandem Adnectin. Once labeled, it was possible to assess its tissue distribution and tumor uptake in xenograft mice. The [^{14}C]-labeled P40B-EI-tandem showed equivalent cellular activity and serum half-life in mice as the nonlabeled version, suggesting that the [^{14}C] label in the linker region does not interfere with the pharmacokinetic and pharmacological properties of the molecule. After dosing [^{14}C]-P40B-EI-tandem to the athymic mice bearing both H292 and RH41 tumors, QWBA showed that the highest uptake of the radioactivity among nontumor tissues was in the liver, followed by the kidneys and lung. The muscle and brain showed the least penetration of the radioactivity among all tissues. In addition, [^{14}C]-P40B-EI-tandem penetrated into the H292 and RH41 tumors, but the extent of accumulation was largely tumor dependent. Collectively, the present study demonstrates the feasibility of applying this new [^{14}C]-labeling method to study the target and tissue distribution of a PEGylated biologic.

Acknowledgments

We gratefully acknowledge the helpful suggestions made by Drs. Huadong Sun, Brad Maxwell, Murli Krishna, and James Bryson (Bristol-Myers Squibb). We also thank Dr. Jochem Gokemeijer (Bristol-Myers Squibb) for providing the exposure data that were first reported by Emanuel et al. (2011).

Authorship Contributions

Participated in research design: H. Wang, L. Wang, Emanuel, Morin, and Bonacorsi.

Conducted experiments: H. Wang, L. Wang, Cao, Lin, Shen, and Hosbach.

Contributed new reagents or analytic tools: Cao.

Performed data analysis: H. Wang, L. Wang, Zhang, and Yang.

Wrote or contributed to the writing of the manuscript: H. Wang, L. Wang, Emanuel, Rodrigues, and Yang.

References

Alagic A, Koprianiuk A, and Kluger R (2005) Hemoglobin-superoxide dismutase-chemical linkages that create a dual-function protein. *J Am Chem Soc* **127:**8036–8043.

Bailon P and Won CY (2009) PEG-modified biopharmaceuticals. *Expert Opin Drug Deliv* **6:**1–16.

Cai W, Chen K, He L, Cao Q, Koong A, and Chen X (2007) Quantitative PET of EGFR expression in xenograft-bearing mice using ^{64}Cu-labeled cetuximab, a chimeric anti-EGFR monoclonal antibody. *Eur J Nucl Med Mol Imaging* **34:**850–858.

Chakrabarti MC, Le N, Paik CH, De Graff WG, and Carrasquillo JA (1996) Prevention of radiolysis of monoclonal antibody during labeling. *J Nucl Med* **37:**1384–1388.

Emanuel SL, Hughes TV, Adams M, Rugg CA, Fuentes-Pesquera A, Connolly PJ, Pandey N, Moreno-Mazza S, Butler J, Borowski V, et al. (2008) Cellular and in vivo activity of JNJ-28871063, a nonquinazoline pan-ErbB kinase inhibitor that crosses the blood-brain barrier and displays efficacy against intracranial tumors. *Mol Pharmacol* **73:**338–348.

Emanuel SL, Engle LJ, Chao G, Zhu RR, Cao C, Lin Z, Yamniuk AP, Hosbach J, Brown J, Fitzpatrick E, et al. (2011) A fibronectin scaffold approach to bispecific inhibitors of epidermal growth factor receptor and insulin-like growth factor-I receptor. *MAbs* **3:**38–48.

Fishburn CS (2008) The pharmacology of PEGylation: balancing PD with PK to generate novel therapeutics. *J Pharm Sci* **97:**4167–4183.

Gaberc-Porekar V, Zore I, Podobnik B, and Menart V (2008) Obstacles and pitfalls in the PEGylation of therapeutic proteins. *Curr Opin Drug Discov Devel* **11:**242–250.

Gay RD, Clarke AW, Elgundi Z, Domagala T, Simpson RJ, Le NB, Doyle AG, and Jennings PA (2010) Anti-TNFα domain antibody construct CEP-37247: full antibody functionality at half the size. *MAbs* **2:**625–638.

Gebauer M and Skerra A (2009) Engineered protein scaffolds as next-generation antibody therapeutics. *Curr Opin Chem Biol* **13:**245–255.

Hoeben BA, Molkenboer-Kuenen JD, Oyen WJ, Peeters WJ, Kaanders JH, Bussink J, and Boerman OC (2011) Radiolabeled cetuximab: dose optimization for epidermal growth factor receptor imaging in a head-and-neck squamous cell carcinoma model. *Int J Cancer* **129:**870–878.

Hopp J, Hornig N, Zettlitz KA, Schwarz A, Fuss N, Müller D, and Kontermann RE (2010) The effects of affinity and valency of an albumin-binding domain (ABD) on the half-life of a single-chain diabody-ABD fusion protein. *Protein Eng Des Sel* **23:**827–834.

Hovgaard D, Mortensen BT, Schifter S, and Nissen NI (1992) Clinical pharmacokinetic studies of a human haemopoietic growth factor, GM-CSF. *Eur J Clin Invest* **22:**45–49.

Hovgaard DJ, Folke M, Mortensen BT, and Nissen NI (1994) Recombinant human interleukin-3: pharmacokinetics after intravenous and subcutaneous bolus injection and effects on granulocyte kinetics. *Br J Haematol* **87:**700–707.

Ishida T and Kiwada H (2008) Accelerated blood clearance (ABC) phenomenon upon repeated injection of PEGylated liposomes. *Int J Pharm* **354:**56–62.

Jevsevar S, Kunstelj M, and Porekar VG (2010) PEGylation of therapeutic proteins. *Biotechnol J* **5:**113–128.

Lipovsek D (2011) Adnectins: engineered target-binding protein therapeutics. *Protein Eng Des Sel* **24:**3–9.

Nayak TK, Garmestani K, Baidoo KE, Milenic DE, and Brechbiel MW (2010a) Preparation, biological evaluation, and pharmacokinetics of the human anti-HER1 monoclonal antibody panitumumab labeled with ^{86}Y for quantitative PET of carcinoma. *J Nucl Med* **51:**942–950.

Nayak TK, Regino CA, Wong KJ, Milenic DE, Garmestani K, Baidoo KE, Szajek LP, and Brechbiel MW (2010b) PET imaging of HER1-expressing xenografts in mice with 86Y-CHX-A″-DTPA-cetuximab. *Eur J Nucl Med Mol Imaging* **37:**1368–1376.

Niu G, Li Z, Xie J, Le QT, and Chen X (2009) PET of EGFR antibody distribution in head and neck squamous cell carcinoma models. *J Nucl Med* **50:**1116–1123.

Sato H (2002) Enzymatic procedure for site-specific pegylation of proteins. *Adv Drug Deliv Rev* **54:**487–504.

Skerra A (2007) Alternative non-antibody scaffolds for molecular recognition. *Curr Opin Biotechnol* **18:**295–304.
Stork R, Campigna E, Robert B, Müller D, and Kontermann RE (2009) Biodistribution of a bispecific single-chain diabody and its half-life extended derivatives. *J Biol Chem* **284:**25612–25619.
Taguchi T (1986) Clinical studies of recombinant interferon alfa-2a (Roferon-A) in cancer patients. *Cancer* **57:**1705–1708.
Tolcher AW, Sweeney CJ, Papadopoulos K, Patnaik A, Chiorean EG, Mita AC, Sankhala K, Furfine E, Gokemeijer J, Iacono L, et al. (2011) Phase I and pharmacokinetic study of CT-322 (BMS-844203), a targeted Adnectin inhibitor of VEGFR-2 based on a domain of human fibronectin. *Clin Cancer Res* **17:**363–371.
Tolmachev V, Rosik D, Wållberg H, Sjöberg A, Sandström M, Hansson M, Wennborg A, and Orlova A (2010) Imaging of EGFR expression in murine xenografts using site-specifically labelled anti-EGFR ^{111}In-DOTA-Z EGFR: 2377 Affibody molecule: aspect of the injected tracer amount. *Eur J Nucl Med Mol Imaging* **37:**613–622.
Veronese FM and Mero A (2008) The impact of PEGylation on biological therapies. *BioDrugs* **22:**315–329.

Address correspondence to: Dr. Haiqing Wang, Metabolism and Pharmacokinetics, Pharmaceutical Candidate Optimization, Bristol-Myers Squibb Research and Development, Route 206 and Province Line Rd., Princeton, NJ 08543. E-mail: haiqing.wang@bms.com